Anomalous breakdown of Bloch's rule in the Mott-Hubbard insulator MnTe_{2}

Tapan Chatterji, Antonio M. dos Santos, Jamie J. Molaison, Thomas C. Hansen, Stefan Klotz, Mathew Tucker, Kartik Samanta, and Tanusri Saha-Dasgupta

Origin of anomalous breakdown of Bloch's rule in the Mott-Hubbard insulator MnTe$_2$

Tapan Chatterji[1], Antonio M. dos Santos[2], Jamie J. Molaison[2],
Thomas C. Hansen[1], Stefan Klotz[3] and Mathew Tucker[4]

[1] *Institut Laue-Langevin, B.P. 156, 38042 Grenoble Cedex 9, France*
[2] *Quantum Condensed Matter Div., Oak Ridge National Laboratory, TN 37831-6460, USA*
[3] *IMPMC, CNRS UMR 7590, Université Pierre et Marie Curie, 75252 Paris*
[4] *ISIS Facility, Rutherford Appleton Laboratory, Chilton, Didcot, UK*

Kartik Samanta[5] and Tanusri Saha-Dasgupta[5]
[5] *Department of Condensed Matter Physics and Materials Science,
S.N. Bose National Centre for Basic Sciences, Kolkata-700098, India.*

(Dated: February 25, 2015)

We reinvestigate the pressure dependence of the crystal structure and antiferromagnetic phase transition in MnTe$_2$ by the rigorous and reliable tool of high pressure neutron powder diffraction. First-principles density functional theory calculations are carried out in order to gain microscopic insight. The measured Néel temperature of MnTe$_2$ is found to show unusually large pressure dependence of 12 K GPa^{-1}. This gives rise to large violation of Bloch's rule given by $\alpha = \frac{d \log T_N}{d \log V} = -\frac{10}{3} \approx -3.3$, to a α value of -6.0 $\pm$ 0.1 for MnTe$_2$. The ab-initio calculation of the electronic structure and the magnetic exchange interactions in MnTe$_2$, for the measured crystal structures at different pressures, gives the pressure dependence of the Neél temperature, α to be -5.61, in close agreement with experimental finding. The microscopic origin of this behavior turns to be dictated by the distance dependence of the cation-anion hopping interaction strength.

PACS numbers: 75.30.Vn, 75.25.+z, 75.40.Cx

I. INTRODUCTION

Long time ago in 1966, Bloch[1] studied the pressure variation of the Néel temperature, T_N and that of volume (V) of several transition-metal (TM) based antiferromagnetic insulators (AFI) and came up with the general relationship

$$\alpha = \frac{d \log T_N}{d \log V} = -\frac{10}{3} \approx -3.3. \qquad (1)$$

In the localized-electron limit where perturbative superexchange theory is applicable, the Néel temperature can be related to the effective TM-TM hopping interaction (b), charge transfer energy (Δ) and Coulomb interaction (U), as

$$T_N \sim b^2 \left[\frac{1}{U} + \frac{1}{2\Delta} \right]. \qquad (2)$$

The first term in the above equation is the Anderson superexchange term and the second term involves the two electron transfer from the anion. A theoretical rationalization of the Bloch's rule comes from the calculations of the variation of the cation-anion transfer integral b^{ca} with the cation-anion bond length r, which varies as r^{-n}. The calculated values[2,3] of n using molecular orbital theory or configuration interaction method on transition-metal oxides and flourides, turn out to be in the range 2.5-3. This leads to $T_N \sim r^{-10} \sim V^{-3.3}$, assuming $b = (b^{ca})^2/\Delta$. Experimentally Bloch's rule is obeyed by a variety of Mott insulators. However, there are exceptions too. For example, while Bloch rule is found to be obeyed in YCrO$_3$

and CaMnO$_3$, it was found to fail in LaMnO$_3$.[4] The failure has been explained in terms of breakdown of localized approach used in Bloch's formulation. We note that the cases discussed so far on the pressure dependence of T$_N$, all involve oxygen or flourine, *i.e.* anions with $2p$ electrons. As is well known, the nature of anionic wavefunction changes as one moves down the column of the periodic table, from $2p$ to $3p$ series and even more to $4p$ and $5p$ series, effecting the TM-anion bonding. It would therefore be of interest to consider the validity of Bloch's criterion in case of TM compounds containing anions like Te.

A compound of interest in this context is MnTe$_2$. MnTe$_2$ belongs to a large class of pyrite type and related marcasite and arsenopyrite type compounds MX$_2$ (M = transition element, X = Chalcogen or pnictogen element) with diverse magnetic and electrical properties. They range from insulator to metal or even superconductor. They can be diamagnetic, weakly paramagnetic, ferromagnetic or antiferromagnetic etc. The magnetic semiconductor MnTe$_2$ having a pyrite type crystal structure, as shown in Fig. 1, orders below $T_N \approx 88$ K in type-I antiferromagnetic structure[5–7] with the propagation vector $\mathbf{k} = (1,0,0)$. The magnetic phase transition at T_N was found to be of second order within experimental resolution[6,7] although the related other manganese dichalcogenides MnS$_2$ and MnSe$_2$ undergo first-order phase transitions[8–11] at T_N. The magnetic structure of MnTe$_2$ had been subject to controversy,[5,12,13] regarding whether the magnetic structure of MnTe$_2$ is of collinear single-$\mathbf{k}$ or non-collinear triple-$\mathbf{k}$ type, or whether there is any spin reorientation transition. Burlet
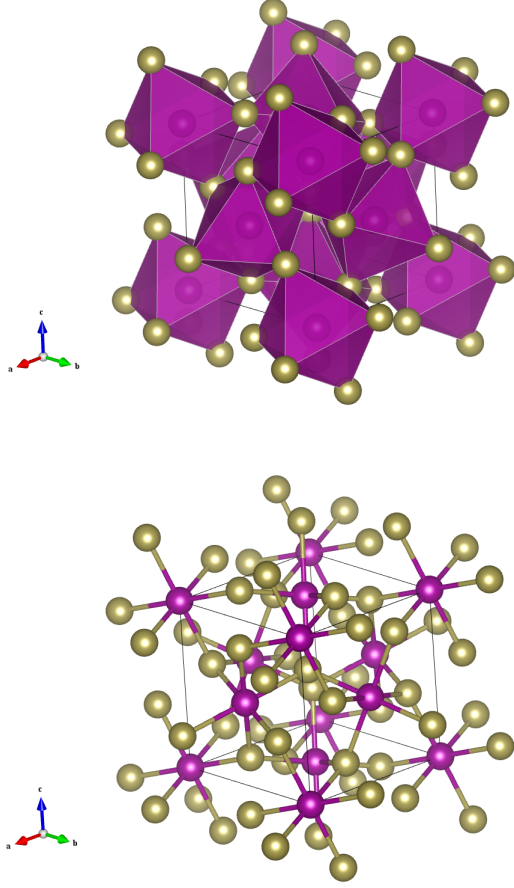
FIG. 1: (Color online) Schematic representation of the crystal structure of MnTe$_2$. Mn atoms are shown as smaller purple spheres and Te atoms as larger yellow spheres. The upper panel shows the polyhedral representation of the MnTe$_6$ octahedra. The lower panel shows the ball and stick version of the same structure where the distorted octahedral coordination of the Mn by six Te atoms and distorted tetrahedral coordination of the Te atom by the three Mn and one Te atoms can be seen.

FIG. 2: (Color online) Pressure dependence of the structural parameters of MnTe$_2$ determined from the data measured on PEARL diffractometer of ISIS Facility. The red continuous lines are guides to the eye.

et al.[7] resolved this controversy and determined the magnetic structure to be of non-collinear triple-**k** type. The structure was found to be stable below T_N down to 4.2 K, the lowest temperature at which the magnetic structure was investigated.

The high pressure X-ray diffraction was carried out previously,[14,15] to study the pressure induced volume changes in MnTe$_2$, though no detailed structural analysis was carried out in terms of determination of atomic positions. Also, in a separate study the pressure dependence of Néel temperature was obtained from resistivity and Mössbauer measurements.[25] The results of these two studies put together show a large violation of Bloch's rule, which however has not been stressed before. More importantly, a microscopic understanding of this phenomena was lacking.
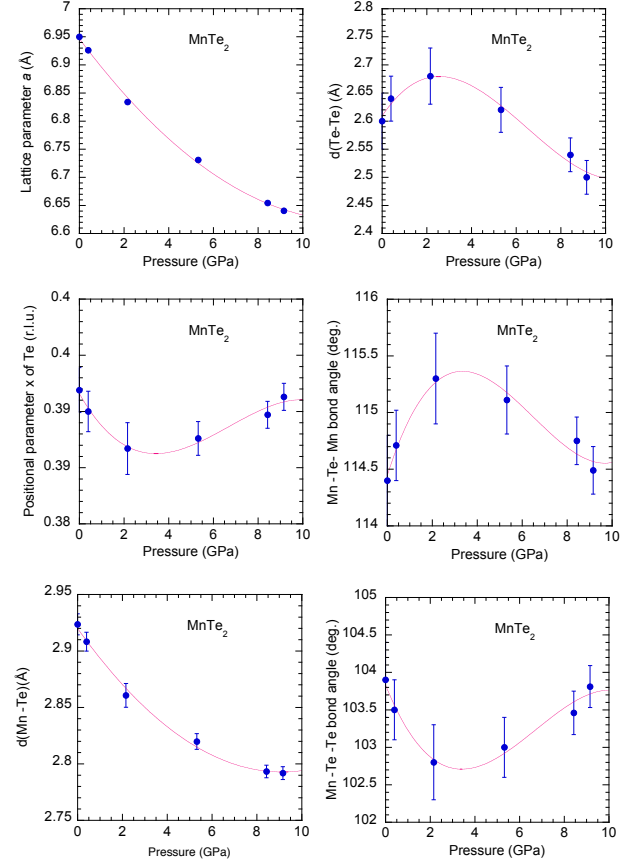
In the present study, we take up this issue by experimentally revisiting the pressure dependence of the structure and magnetic ordering temperature of MnTe$_2$ in terms of high-pressure powder neutron diffraction measurment, together with first-principles density functional theory (DFT) calculation to provide the microscopic understanding. The neutron diffraction study carried out in the present work, is undoubtedly a more reliable tool to measure the magnetic transition temperatures, compared to resistivity or Mössbauer. In addition, the present neutron diffraction study provide the detailed structural information, which was not available before, based on which our first-principles calculations have been carried out. Our rigorous study confirms and rationalizes the breakdown of Bloch's rule in MnTe$_2$.
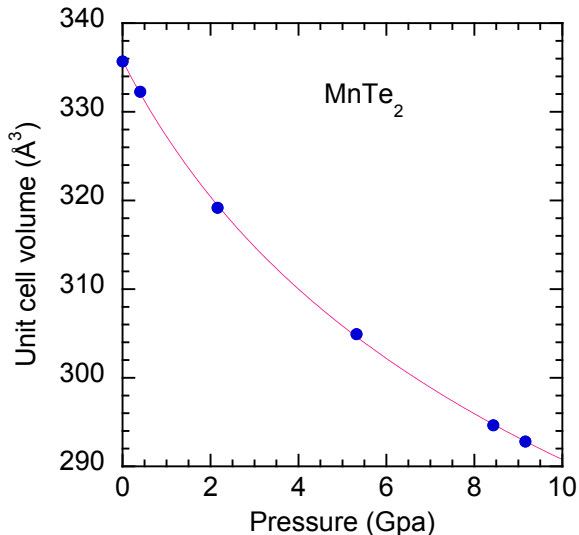
to 77 K was achieved by flooding the cell assembly with liquid N_2. The pressure was determined from the known pressure variation[14,15] of the lattice parameter of $MnTe_2$.

DFT calculations on the experimentally measured structures were carried out in the plane-wave basis, within the generalized gradient approximation (GGA) for the exchange-correlation functional, as implemented in the Vienna Ab-initio Simulation Package.[22] We used Perdew-Burke-Ernzerhof implementation of GGA.[23] The projector augmented wave potential was used. For the total energy calculation of different spin configurations, we considered a $2 \times 2 \times 1$ super-cell containing a total of 48 atoms in the cell. For the self-consistent field calculation, an energy cut-off of 600 eV and $4 \times 4 \times 8$ Monkhorst-pack K-point mesh were found to provide good convergence of the total energy. The missing correlation at the Mn sites beyond GGA, was taken into account through supplemented Hubbard U (GGA+U) calculation[24] following the Dudarev implementation, with choice of $U = 5.0$ eV and Hund's coupling, J_H of 0.8 eV. Variation in U value has been studied and found to have no significant effect on the trend.

III. EVOLUTION OF THE STRUCTURAL PARAMETERS UNDER PRESSURE

The pyrite type crystal structure of $MnTe_2$ in the $Pa\bar{3}$ space group has Mn atom at $4(a)$ (000) and Te atom at $8(c)$ (xxx) position. The cubic lattice parameter a and the Te positional parameter x were refined along with the isotropic atomic displacement parameters of Mn and Te atoms. Figure 2 shows the pressure dependence of the structural parameters of $MnTe_2$, viz. lattice parameter, positional parameter x of Te atom, Mn-Te and Te-Te bond lengths and the Mn-Te-Mn and Mn-Te-Te bond angles. The results are very remarkable and contrary to our naive expectation that the Te-Te bond distance would continuously decrease with pressure. Instead the bond distance seems to increase slightly at lower pressure but after reaching a maximum at P = 2 GPa it decreases and becomes somewhat flat at about P = 10 GPa. The two bond angles also show anomalous pressure dependence. This is expected since all the relevant bond distances and angles are derived from the single Te positional parameter x and the cubic lattice parameter a that decreases with pressure in the usual way. In contrast, the Mn-Te bond length is highly pressure sensitive and almost entirely responsible for the pressure-induced volume reduction, suggesting relatively weak Mn -Te bonds which are susceptible to changes upon application of pressure. The remarkable pressure response of the Te-Te bond distance and Mn-Te-Mn and Mn-Te-Te angles should be reflected in the pressure dependence of the superexchange interaction that decides the pressure variation of the Néel temperature, as obtained in our first-principles calculations. Fig. 3 shows the pressure variation of the unit cell volume of $MnTe_2$ and its fit with Murnaghan equa-

FIG. 3: (Color online) Pressure variation of the unit cell volume of $MnTe_2$ and its fit with Murnaghan equation of state that gives $B_0 = 34.6 \pm 1.0$ GPa and $Bo' = 8.8 \pm 0.4$.

II. METHODOLOGY

High pressure neutron diffraction investigations were done on three neutron powder diffractometers, viz. PEARL at the ISIS Facility in UK, D20 of Institute Laue-Langevin, Grenoble and also SNAP at SNS, Oak Ridge. Pressure was generated by Paris-Edinburgh pressure cells[19,20] and a mixture of 4:1 deuterated methanol:ethanol was used as pressure transmitting medium. The PEARL measurements used anvils made of tungsten carbide and a scattering geometry which restricted the available d-spacing range to below 4.2 $\mathring{A}$, i.e. the magnetic (100) reflection was not recorded. Rietveld refinements of the patterns to the crystal structure were carried out by the GSAS program[21]. The experiments on D20 and SNAP used anvils made of cubic boron nitride[20] and a scattering geometry which gives access to reflections with larger d-spacings. The sample temperature was controlled using closed-cycle cryostats; fast cooling
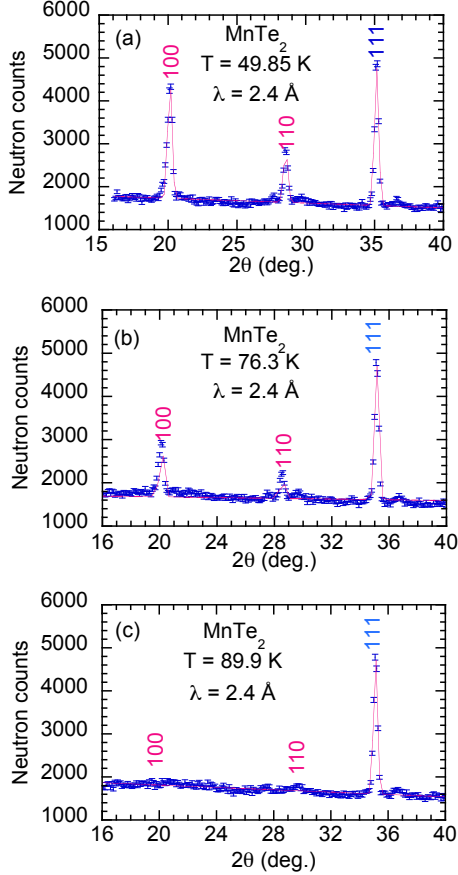
FIG. 4: (Color online) Neutron powder diffraction intensities of the 100 and 110 magnetic peaks along with the 111 nuclear peak at several temperatures below and close to the antiferromagnetic Néel temperature $T_N = 88$ K. The data have been measured on the D20 diffractometer of the Institut Laue-Langevin in ambient pressure. The red lines are results of Gaussian fits of the Bragg peaks.

tion of state. The fit gave $B_0 = 34.6 \pm 1.0$ GPa and $Bo' = 8.8 \pm 0.4$ where B_0 is the bulk modulus and Bo' is its pressure derivative. The values agree well with the values determined previously from high pressure X-ray diffraction[14,15].

IV. MEASURED PRESSURE VARIATION OF $\mathbf{T}_N$

The antiferromagnetic phase transition of MnTe$_2$ was first investigated at ambient pressure with the sample (outside the pressure cell) fixed to the cold tip of the standard orange cryostat. Fig. 4 shows neutron powder diffraction intensities of the 100 and 110 magnetic peaks along with the 111 nuclear peak at several temperatures
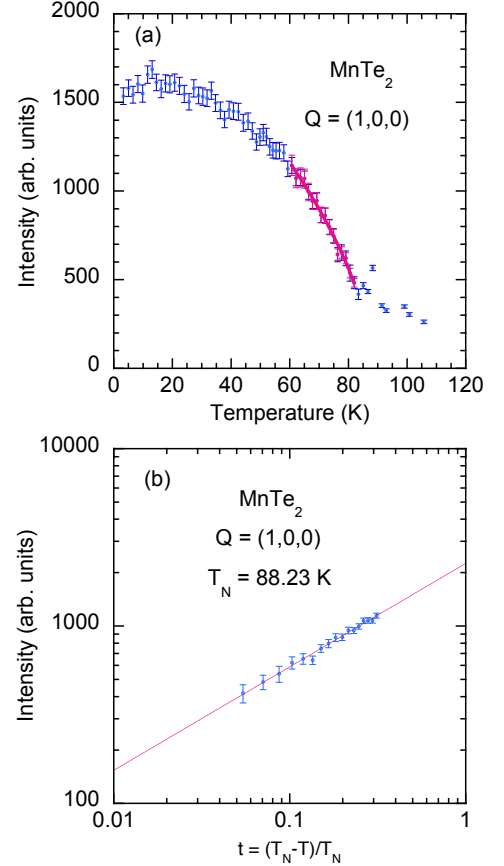

FIG. 5: (Color online) (a) Temperature variation of the integrated intensitiy of the 100 magnetic Bragg peak. The red line is result of the least-squares fit of the data. The temperature range of the data used for the fit is also given by the temperature range of the red line. The least-squares fit gives the power-law exponent $\beta = 0.29 \pm 0.04$ and a Néel temperature $T_N = 88 \pm 2$ K. (b) Log-log plot of the intensity of the 100 magnetic reflection vs. reduced temperature.

below and close to the antiferromagnetic Néel temperature $T_N = 88$ K. Fig. 5(a) shows the temperature variation of the integrated intensity of the 100 magnetic Bragg peak. The intensity of this reflection decreases continuously with increasing temperature and becomes zero at about $T_N \approx 88$ K. The data just below T_N could be fitted by a power-law exponent

$$I = I_0 \left(\frac{T_N - T}{T_N} \right)^{2\beta} \qquad (3)$$

where I is the integrated intensity, I_0 is the saturation value of the intensity at $T = 0$, T_N is the critical temperature and β is the power-law exponent. Least-squares fit of the data in the temperature range from $T = 60$ to $T = 88$ K gave $\beta = 0.29 \pm 0.04$ and a Néel temperature
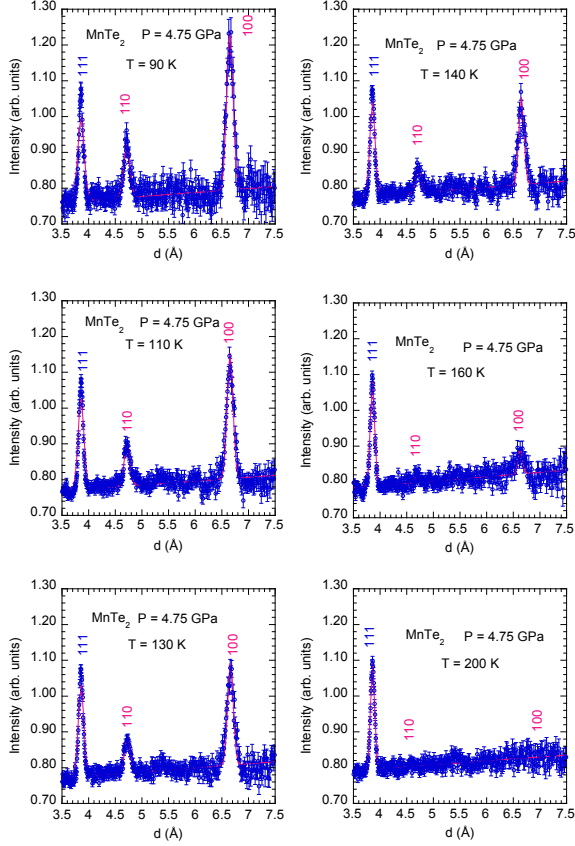
FIG. 6: (Color online) Neutron powder diffraction intensities of the 100 and 110 magnetic peaks along with the 111 nuclear peak of MnTe$_2$ under $P = 4.75$ GPa at several temperatures below and above the antiferromagnetic Néel temperature measured on the SNAP diffractometer of the SNS of Oak Ridge National Laboratory. The red lines are results of Gaussian fits of the Bragg peaks.

$T_N = 88 \pm 2$ K. The fitted value of the Néel temperature was used to determine the reduced temperature $t = (T_N - T)/T_N$. We then produced a standard log-log plot shown in Fig. 5 (b) to extract the critical exponent $\beta = 0.29$ from the slope that agreed well with that determined by the least-squares fit.

Fig. 6 shows neutron powder diffraction intensities of the 100 and 110 magnetic peaks along with the 111 nuclear peak of MnTe$_2$ under $P = 4.75$ GPa at several temperatures below and above the antiferromagnetic Néel temperature. It is immediately noticed that the application of hydrostatic pressure P = 4.75 GPa increases the Néel temperature $T_N = 88$ K of MnTe$_2$ substantially. By fitting the temperature dependence of the intensity of the 100 magnetic peak and fitting the data by a power law we determine $T_N = 145 \pm 7$ K. Fig. 7(a) shows
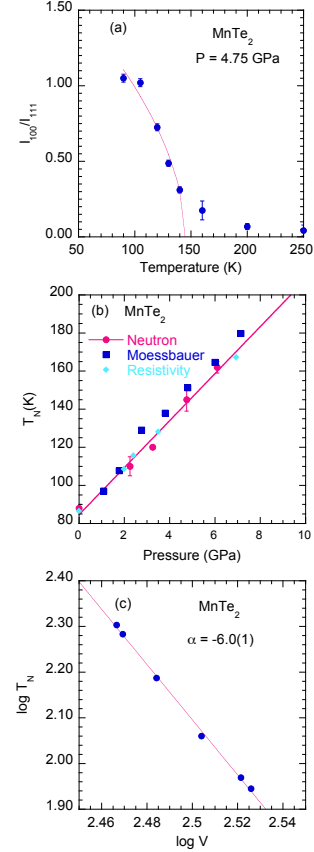
FIG. 7: (Color online) (a) Temperature variation of the intensity of the 100 reflection of MnTe$_2$ at $P = 4.75$ GPa and its power-law fit. The red line is result of the least-squares fit of the data. The power law fit yields $T_N = 145 \pm 7$ K. (b) Pressure variation of the Néel temperature of MnTe$_2$. The Mössbauer and the resistivity data are taken from Vulliet et al.[25]. The linear fit of the neutron data yields $\frac{dT_N}{dP} = 12$ K GPa^{-1}. (c) Log-log plot of Néel temperature T$_N$ vs. unit cell volume of MnTe$_2$. The red straight line is the result of the linear fit of the data yielding $\alpha = -6.0 \pm 0.1$.

this fit. Similarly we determined the Néel temperatures of MnTe$_2$ at several pressures. The result is shown in Fig. 7(b). The obtained trend agrees well with that obtained from resistivity and Mössbauer spectroscopy[25], as also shown in Fig. 7(b). The neutron diffraction results show that T_N of MnTe$_2$ increases linearly in the pressure range $0 - 8$ GPa at a rate of about 12 K GPa^{-1}, determined from the slope of the linear plot. From this linear relationship we calculated the T$_N$ values for the pressures at which we determined the lattice and positional parameters of MnTe$_2$ from the high pressure neutron diffraction experiment on the PEARL diffractometer. Fig. 7(c) shows the log-log plot of Néel temperature

T_N vs. unit cell volume of $MnTe_2$. The slope of this plot gives $\alpha = -6.0 \pm 0.1$ which is much larger than the Bloch rule value of $\alpha = -3.3$. Our result therefore point towards a spectacular breakdown of Bloch's rule in $MnTe_2$. We note that transition to a non-magnetic state of the Mn^{2+} ions in $MnTe_2$ was reported[25] from the resistivity and Mössbauer study, and also evidenced by the pressure variation of infrared reflectivity investigated by Mita et al.[26]. Our experiments however did not show the volume collapse observed in high pressure X-ray diffraction experiments[14,15]. It is therefore plausible that we did not reach the transition pressure during the present high pressure neutron diffraction experiments. The exact pressure at which the transition to a non-magnetic state is expected to happen depends sensitively on the experimental conditions.

The present neutron diffraction data contain in principle the magnetic moment information because neutron diffraction probes both crystal and the magnetic structures and the intensities of the magnetic reflections when put to the absolute scale by using the intensities of the nuclear reflections can give the ordered moment values. However this is not an easy task especially in a high pressure experiment using a large Paris-Edinburg pressure cell. The high absorption of the pressure cell and also a very high background hinders accurate determination of the nuclear and magnetic intensities. In the present case despite our efforts the determination of the pressure dependence of ordered moment from the neutron diffraction data was not successful. We know however from our calculations (using pressure dependence of the structural parameters) that the ordered moment of Mn ions does not change at all (or very little) in the range 0 - 9 GPa investigated. The present high pressure neutron diffraction data seem to support this result. The intensity ratio of the magnetic and nuclear Bragg peaks do not change very much and is within the accuracy in the pressure range investigated.

V. FIRST-PRINCIPLES STUDY

A. Calculated Pressure Variation of Neél Temperature

To gain understanding on the significantly large pressure dependence of the Neél temperature in $MnTe_2$ we carried out theoretical investigation in terms of first-principles DFT calculations. Fig. 8 shows the comparison of the spin-polarized density of states of $MnTe_2$ at ambient pressure and at a pressure of 9.16 GPa, the highest pressure studied in the present calculations. The spin-polarized calculations within GGA+U gave rise to a magnetic moment of 4.6 μ_B (4.5 μ_B) at Mn site together with a moment of 0.03 μ_B (0.05 μ_B) at Te site
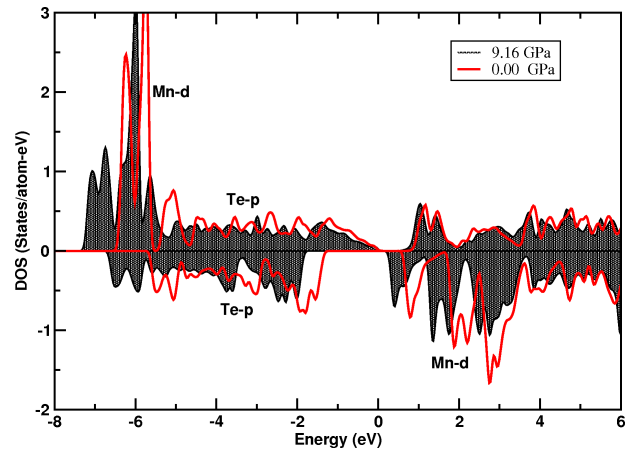

FIG. 8: (Color online) Comparison of GGA+U density of states between the ambient pressure (solid line) and high pressure (shaded area) phases. The energies are measured with respect to GGA+U Fermi energy. The states of dominant Mn-d and Te-p characters have been marked.

for the ambient (P = 9.16 GPa) pressure condition, suggesting the high-spin state of Mn at both ambient and high pressure conditions, in agreement with experimental findings. Both ambient pressure and high pressure phases were found to be insulating, with a gap at Fermi energy, marked as zero in the figure. The Mn-d states are fully occupied in the majority spin channel and completely empty in minority spin channel, in correspondence with high spin state of Mn in its nominal 2+ valence state. The comparison of the density of states between ambient pressure and at high pressure though, shows enhancement of the Mn-d band width by ≈ 1 eV, indicating the hopping interaction between Mn-d and Te$-p$ to increase substantially in moving from ambient to high pressure phase.

To extract the various magnetic interactions (J's) between the Mn spins, we calculated the GGA+U total energies for various configurations of Mn spins and mapped the total energy onto an underlying S = 5/2 Heisenberg model. Calculations were carried out for six different pressures, 0.0 GPa, 0.4 GPa, 2.16 GPa, 5.32 GPa, 8.43 GPa and 9.16 GPa. The dominant magnetic interactions considered in our calculation of J's, were J_1, between the first nearest neighbor (1NN) Mn atoms, connected to each other by the corner-shared Te atoms, and J_2, between the second nearest neighbor (2NN) Mn atoms, connected to each other through Te-Mn-Te bridges.

Apart from the ferromagnetic (FM) configuration, with all Mn spins in the supercell pointing in the same direction, two different antiferromagnetic (AFM) configurations, AFM1 and AMF2 were considered, with antiferromagnetic arrangement of 1NN Mn and 2NN Mn spins. The GGA+U total energies corresponding to AFM configurations, measured with respect to the energy of FM configuration, turned out to be negative, for all the studied pressures, in accordance with dominance
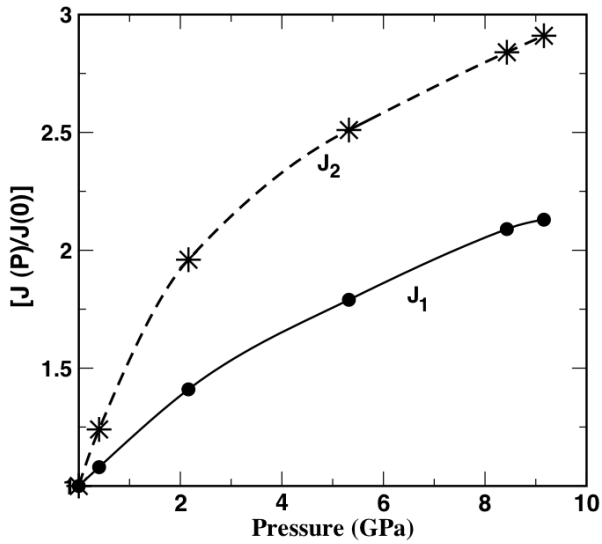
FIG. 9: The ratio of J's at pressure P and that at ambient pressure (denoted as P = 0), plotted as a function of pressure. The solid line corresponds to J_1, and dashed line corresponds to J_2.

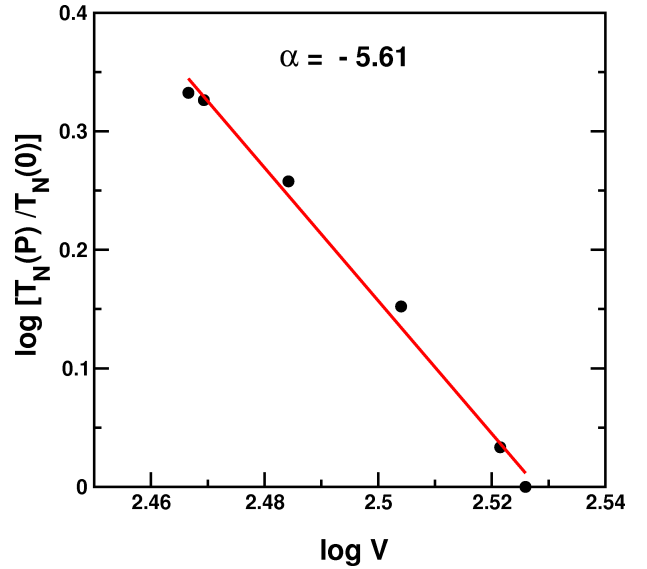

FIG. 10: (Color online) Log-log plot of $T_N(P)/T_N(0)$ versus volume. The linear fit to the data points is shown with line, having a slope of α = -5.61.

of anti-ferromagnetic interactions. Extracting J_1 and J_2 by mapping the total energy onto the spin Hamiltonian, given by $H = -J_1 \sum_{nn} S_{Mn}^i . S_{Mn}^j - J_2 \sum_{2nn} S_{Mn}^i . S_{Mn}^j$, gave J_2 a small fraction of J_1, with $J_1/J_2 = 0.09$ at ambient pressure and 0.12 at 9.16 GPa, suggesting the magnetism being primarily governed by J_1. The pressure dependence of exchange interactions is shown in Figure 9.

With the knowledge of J's, we calculated the Neél temperature T_N using Mean-field theory, given by $T_N^{mf} = \frac{S(S+1)J_0}{3K_B}$, where J_0 is the net effective interaction $12J_1 + 4J_2$, S = 5/2, and K_B is the Boltzmann constant. Mean field is expected to overestimate the transition temperature, though the trend is expected to captured well, which is governed by J's. The computed $\log[T_N(P)/T_N(0)]$ plotted as a function of $\log(V)$ is shown in Fig. 10. The straight line fit to the calculated data points gives rise to a slope of -5.61, close to the experimental estimate of -6.0 ± 0.1. Both our experimental results and ab-initio calculations, thus establish that Bloch's rule is largely violated in MnTe$_2$. In the following we theoretically investigate the microscopic origin of this behavior.

B. Microscopic Origin of breakdown of Bloch rule

Bloch's rule has been found to be very successful with many magnetic insulators, especially the transition metal oxides and fluorides. The question then arises: what makes the Bloch's rule fail for MnTe$_2$? In order to explore this, we extracted the hopping interactions b^{ca}, where

c and a signifies Mn and Te, respectively, by carrying out N-th order muffin-tin orbital (NMTO) based NMTO-downfolding calculations.[27] This involved construction of real-space representation of the Mn d- O p Hamiltonian in Wannier function basis out of the full DFT calculations, by integrating out all the degrees of freedom other than Mn d and Te p. Our NMTO-downfolding calculations to extract the dependence of b^{ca} on cation-anion distance r gave, $b^{ca} \sim \frac{1}{r^{4.2}}$, instead of $b^{ca} \sim \frac{1}{r^{2.5}}$ assumed for derivation of the Bloch's rule. This gives $T_N \sim \frac{1}{r^{17}} \sim \frac{1}{V^{5.67}}$, very close to the estimate obtained from total energy calculations, as well as from the experiment. This points to the fact that violation of Bloch's rule in case of MnTe$_2$ is caused due to the deviation in the distance dependence of b^{ca}, from the $\frac{1}{r^{2.5}}$ behavior rather than that by U or Δ. We find that the distance dependence of b^{ca} found for MnTe$_2$, is more like the canonical behaviour,[28] in which the interatomic matrix elements are supposed to scale with distance as $\frac{1}{r^{l+l'+1}}$ where l and l' are the angular momenta of the orbitals involved. In case of several TM oxides, on the other hand, anaalysis of DFT band structure,[29] gave rise to a $\frac{1}{r^{l+l'}}$ behavior, similar to that obtained from molecular orbital theory or configuration interaction method on KNiF$_4$ or MnO or MnF$_2$[2,3]. This presumably originates from differential nature of Te $4p$ wavefunctions compared with that of $2p$ or $3p$, which together with non monotonic pressure dependence of position parameter, x, influences the super-exchange interaction in a differential manner.

VI. SUMMARY

In conclusion, the Néel temperature of MnTe$_2$ was found to show unusually large pressure dependence of

about 12 K GPa^{-1}, which has been confirmed in the present study through more rigorous and reliable high pressure neutron diffraction experiments compared to that in literature, as well as through first-principles density functional theory calculations. Our measured pressure dependence of the Néel temperature and unit cell volume gave $\alpha = -6.0 \pm 0.1$ which is much larger than that expected from the Bloch's rule $\alpha = \frac{d \log T_N}{d \log V} = -\frac{10}{3} \approx -3.3$. The calculated pressure dependence of Néel temperature gave rise to $\alpha = -5.61$ in good agreement with the experimental estimate. We provided a microscopic understanding of this behavior in terms of the distance dependence of Mn-Te hopping interaction upon application of pressure, which showed significant deviation from that for NiF_4 or MnO or MnF_2[2,3].

Finally, the large pressure dependence of magnetic interactions and magnetic ordering temperature provide us with a handle to tune the properties of magnetic materials, which can lead to important technological applications. The present study, should have important bearing on this topic.

[1] D. Bloch, J. Phys. Chem. Solids **27**, 881 (1966).

[2] D.W. Smith, J. Chem. Phys., **50**, 2784 (1969).

[3] K.N. Shrivastava and V. Jaccarino, Phys. Rev. B **13**, 299 (1976).

[4] J.-S. Zhou and J.B. Goodenough, Phys. Rev. Lett. **89**, 087201-1 (2002).

[5] J.M. Hastings, N. Elliott, and L.M. Corliss, Phys. Rev. **115**, 13 (1959).

[6] T. Chattopadhyay, and H. Fjellvag, Phys. Lett. A **120**, 44 (1987).

[7] P. Burlet, E. Ressouche, B. Malaman, R. Welter, J.P. Sanchez, and P. Vulliet, Phys. Rev. B **56**, 14013 (1997).

[8] J.M. Hastings, and L.-M. Corliss, Phys. Rev. B **14**, 1995 (1976).

[9] T. Chattopadhyay, H.G. von Schnering, and H.A. Graf, Solid State Comm. **50**, 865 (1984).

[10] T. Chattopadhyay, T. Brückel and P. Burlet, Phys. Rev. B **44**, 7394 (1991).

[11] T. Chattopadhyay, J. Rossat-Mignod and H. Fjellvåg, Solid State Comm., **63**, 65 (1987).

[12] M. Pasternak and A.M. Spijkervet, Phys. Rev. B **181**, 574 (1969).

[13] J.M. Hastings, L.M. Corliss, M. Blume, and M. Pasternak, Phys. Rev. B **1**, 3209 (1970).

[14] H. Fjellvåg, A. Kjekshus, T. Chattopadhyay, H.D. Hochheimer, W. Hönle and H.G. von Schnering, Phys. Lett. **112A**, 411 (1985).

[15] H. Fjellvåg, W.A. Grosshans, W. Hönle and A. Kjekshus, J. Magn. Magn. Mat. **145**, 118 (1995).

[16] T. Chattopadhyay and H.G. von Schnering, J. Phys. Chem. Solids **46**, 113 (1985).

[17] T. Chattopadhyay, H.G. von Schnering and W.A. Grosshans, Physica B **139&140**,305 (1986).

[18] S.A.J. Kimber, A. Salamat, S.R. Evans, H.O. Jeschke, K. Muthukumar, M. Tomić, F. Salvat-Pujol, R. Valenti, M.V. Kaisheva, I. Zizak and T. Chatterji, Proc. Nat. Acad. Sci. **111**, 5106 (2014).

[19] J. M. Besson, R. J. Nelmes, G. Hamel, J. S. Loveday, G. Weill, and S. Hull, Physica B **180&181**, 907 (1992).

[20] S. Klotz, Th. Strässle, G. Rousse, G. Hamel and V. Pomjakushin, Appl. Phys. Lett. **86**, 031917 (2005).

[21] R. B. von Dreele and A. C. Larson, Los Alamos National Laboratory Report No. LAUR 86-746, 1986

[22] G. Kresse and J. Hafner, Phys. Rev. B **47**, R558 (1993); G. Kresse and J. Furthmüller, Phys. Rev. B **54**, 11169 (1996).

[23] J. P. Perdew, K. Burke, and M. Ernzerhof, Phys. Rev. Lett. **77**, 3865 (1996).

[24] S. L. Dudarev, G. A. Botton, S. Y. Savrasov, C. J. Humphreys, and A. P. Sutton, Phys. Rev. B **57**, 1505 (1998).

[25] P. Vulliet, J.P. Sanchez, D. Braithwaite, M. Amanowicz and B. Malaman, Phys. Rev. B **63**, 184403-1 (2001).

[26] Y. Mita, Y. Ishida, M. Kobayashi and S. Endo, Acta Physica Polonica A **113**, 617 (2008).

[27] O. K. Andersen, and T. Saha-Dasgupta, Phys. Rev. B **62**, R16219 (2000).

[28] O. K. Andersen, W. Klose, and H. Nohl, Phys. Rev. B **17**, 1209 (1978).

[29] P. Mahadevan, N. Shanthi, and D. D. Sarma, Phys. Rev. B **54**, 11199 (1996).